Nano-sized formazan analogues: Synthesis, structure elucidation, antimicrobial activity and docking study for COVID-19

Huda K. Mahmoud [a], Basim H. Asghar [b], Marwa F. Harras [c], Thoraya A. Farghaly [a,b,*]

[a] *Department of Chemistry, Faculty of Science, Cairo University, Giza 12613, Egypt*
[b] *Department of Chemistry, Faculty of Applied Science, Umm Al-Qura University, Makkah, Saudi Arabia*
[c] *Department of Pharmaceutical Chemistry, Faculty of Pharmacy (Girls), Al-Azhar University, Cairo, Egypt*

ARTICLE INFO

ABSTRACT

Three series of nanosized-formazan analogues were synthesized from the reaction of dithiazone with various types of α-haloketones (ester and acetyl substituted hydrazonoyl chlorides and phenacyl bromides) in sodium ethoxide solution. The structure and the crystal size of the new synthesized derivatives were assured based on the spectral analyses, XRD and SEM data. The antibacterial and antifungal activities were evaluated by agar diffusion technique. The results showed mild to moderate antibacterial activities and moderate to potent antifungal activities. Significant antifungal activities were observed for four derivatives **3a**, **3d**, **5a** and **5g** on the pathogenic fungal strains; *Aspergillus flavus* and *Candida albicans* with inhibition zone ranging from 16 to 20 mm. Molecular docking simulations of the synthesized compounds into leucyl-tRNA synthetase editing domain of *Candida albicans* suggested that most formazan analogues can fit deeply forming stable complexes in the active site. Furthermore, we utilized the docking approach to examine the potential of these compounds to inhibit SARS-CoV-2 3CLpro. The results were very promising verifying these formazan analogues as a hopeful antiviral agents.

1. Introduction

According to World Health Organization (WHO) reports, the misuse of the antibiotics have led to development of Multidrug Resistance among various strains of microorganisms [1]. Accordingly, new antimicrobial agents acting on novel targets have to be developed to overwhelm the increased incidence of microbial resistance to antibiotic remedy. From the best validated antimicrobial targets are the aminoacyl-tRNA synthetase enzymes which are key enzymes in the protein translation, producing the charged tRNAs required for proper assembly of peptide chains. From these enzymes, LeuRS have been considered as a drug target in fungi and bacteria, it is reported to be inhibited in the editing site by the potent antifungal 5-fluoro-1,3-dihydro-1-hydroxy-2,1-benzoxaborole (AN2690) which is in clinical phases [2-4].

Recently, the outbreak of COVID-19, a new coronavirus pneumonia, caused by a new coronavirus (SARS-CoV-2) has emerged as a pandemic according to WHO in March 2020 [5]. To date, millions of infections and thousands of deaths have been recorded all over the world. In this scenario, there is a crucial need for developing antiviral agents interfering with the life cycle of the virus or with the virus replication or membrane fusion [6]. Many researchers have considered the SARS-CoV-2 major protease (Mpro), in addition called chymotrypsin-like protease (3CLpr-2) as a potential target to anti-COVID-19 drugs [7-9].

Literature survey demonstrates that a lot of formazans have been described to possess broad spectrum of biological activities and pharmacological applications [10] such as antimicrobial [11-14], antiviral [15-17], anticancer [18], and anti-inflammatory [19,20].

As for instance, the formazan derivative **I** was reported to display 100% inhibition of the Ranikhet diseases virus [21]. Additionally, the two formazans **II** and **III** synthesized by Misra and Dhar [22] showed 87% and 83% protections against the Ranikhet disease virus, respectively. Furthermore, many formazans **IV** were reported by Lakshmi *et al.* [23] to have significant antibacterial and antifungal activities. Also, Uraz *et al.* [24] synthesized some formazan derivatives **V**, **VI** with different substituents and evaluated their antibacterial and antifungal activities against some selected microorganism species. The results revealed high activity against *C. tropicalis*, *C. kefir*, *S. cerevisiae* and *C. neofarmans* (Fig. 1). Recently, the synthesized drugs in the nanoscale have demonstrated a superior ability to penetrate the DNA of various diseases, which have increased their biological activity and their ability to inhibit the diseases [25,26].

Inspired by the promising previously reported antimicrobial and antiviral activities of formazans and the urgent need of new effective antimicrobial agent and antiviral drugs to act mainly against COVID-19 and in continuation of our research work in synthesis of bioactive compounds [27-32], we synthesized herein a new series of nano-sized formazan analogues to study their potential as antibacterial and antifungal agents *in vitro*. Additionally, molecular docking simulations were done to propose their mode of binding in the editing domain of LeuRS and to show the possibility of these compounds to act against SARS-CoV-2 main protease enzyme.

2. Results and discussion

2.1. Chemistry

The first series of formazan analogues **3a-f** were synthesized in sodium ethoxide solution at room temperature with continuous stirring from dithiazone **1** and ester-hydrazonoyl chlorides **2a-f** (Scheme 1). The structure of the formed s-substituted-dithiazone derivatives **3a-f** (Formazan analogues) were confirmed based on studying their spectral data. Figs. 2 and 3 are examples for IR(**3b**) and ^{1}H NMR(**3a**) of the synthesized series **3a-f**. For instance, IR spectra of the formazan analogues **3a-f** revealed the appearance of two NH-absorption bands at $\nu = 3525$–3410 & 3425–3178 cm^{-1} as well as the characteristic bands at $\nu = 1743$–1671 cm^{-1} refer to the carbonyl group of COOEt. Furthermore, the ^{1}H NMR of all formazan analogues **3a-f** were decorated with the triplet (CH$_3$) and quartet (CH$_2$) signals for the ester COOEt protons and the two NH groups at $\delta = 9.09$–8.56 and 8.78–7.36 ppm in addition to the aliphatic and aromatic protons remarked for each derivatives. The calculated molecular weight for all s-substituted-dithiazones **3a-f** were in agreement with the appeared molecular ion peaks in their mass spectra.

Under similar reaction conditions in sodium ethoxide solution another series of formazan analogues **5a-h** have been synthesized from the reaction of dithiazone **1** and acetyl-hydrazonyl chlorides **4a-h** (Scheme 2). The structure of the prepared formazan analogues **5a-h** were confirmed depending on studying the information derived from their spectroscopic analyses. For instance, IR spectra of the formazan

analogues **5a-h** revealed the appearance of broad absorption band refer to the two NH near $\nu \approx 3450$ cm^{-1} in addition to the absorption band for the C=O near $\nu \approx 1660$ cm^{-1}. Another spectra as ^{1}H NMR for derivatives **5a-h** showed all characteristic signals for the aliphatic and the aromatic protons as indicated in experimental part.

Another two derivatives of formazan analogues **7a,b** were formed through the substitution reaction of dithiazone **1** with phenacyl bromide derivatives **6a,b** on stirring at ordinary temperature in sodium ethoxide solution (Scheme 3). The structure of derivatives **7a,b** were demonstrated based on the spectral data and elemental CHN-analyses as documented in the experimental part. The IR and ^{1}H NMR of derivative **7a** were illustrated in Figs. 4 and 5.

2.2. XRD and SEM analysis

The XRD diffraction is a good tool to predict the size of the solid sample and the degree crystal regularity. Five sample **3d**, **3f**, **5g**, **5h** and **7b** of the synthesized formazan analogues were screened over $10° < 2\theta < 80°$ range to determined their crystallographic features (Figs. 6a-e). All investigated formazan analogues revealed sharp peaks which indicated the crystalline feature of them. The size of the crystals of the five samples was calculated according to the reported Debye–Scherrer equation [33] and the calculated size was tabulated in Table 1. The results referred to the formazan analogues moieties synthesized in the nanometer-scale. In addition, SEM is another tool useful to give excellent insight about the crystallinity as well as surface topography for the tested solid samples. Fig. 7 contains two SEM images for two formazan analogues **5h** and **7b** as examples for the prepared series. The two images indicated that the crystals of the two derivatives are found in the nanometer-scale.

2.3. Antimicrobial activity

Antimicrobial activities were carried out at the Regional Center for Mycology and biotechnology (RCMB), Al-Azhar University, Cairo, Egypt. Target compounds **3a-e**, **5a-h**, **7b** were evaluated for their *in vitro* antibacterial, and antifungal activities, by inhibition zone method
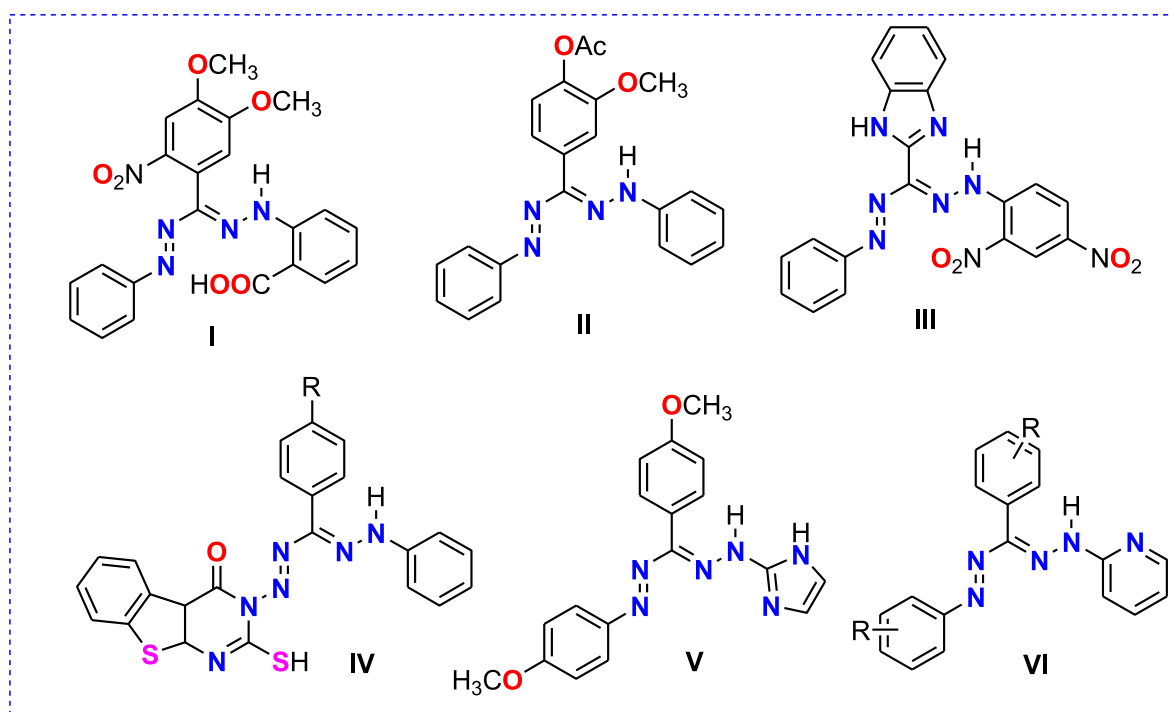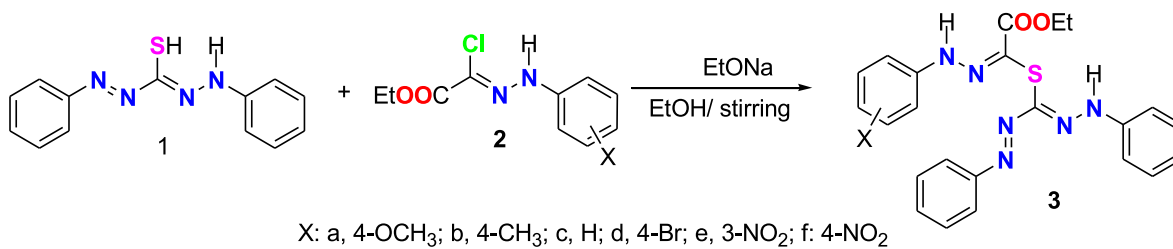

Fig. 1. Some reported antiviral and antimicrobial formazans.

Scheme 1. The reaction of dithiazone **1** with ester hydrazonoyl chlorides **2a-e**.

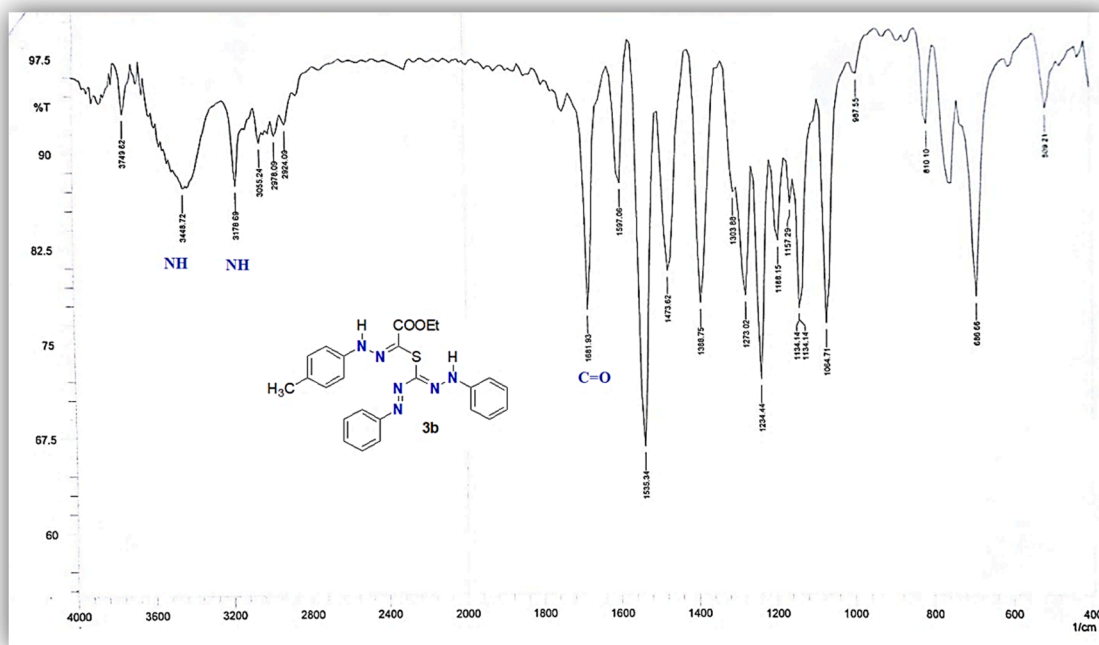X: a, 4-OCH$_3$; b, 4-CH$_3$; c, H; d, 4-Br; e, 3-NO$_2$; f: 4-NO$_2$

Fig. 2. The IR spectrum of derivative **3b**.

against two gram-positive bacteria: *Staphylococcus aureus* (RCMB 010010) and *Bacillus subtilis* (RCMB 015), two gram-negative bacteria: *Escherichia coli* (RCMB 010052) and *Proteus vulgaris* (RCMB 004) and two fungi: *Aspergillus flavus* (RCMB 002002) and *Candida albicans* (RCMB 005003) using gentamycin and ketoconazole as reference antibacterial and antifungal drugs, respectively (Tables 2 and 3).

2.3.1. Antibacterial activity

Concerning the antibacterial activity against gram-positive bacteria, most compounds showed mild to moderate activities. The best activities were seen for the acetyl derivatives **5a**, **5b**, **5c**, **5g** and **5h** with inhibition zones values ranging from 15 to 18 mm, compared to gentamycin with IZ = 24 and 26 mm for *S. aureus* and *B. subtilis*, respectively.

Regarding gram-negative bacteria, they were resistant to **3a** and **3b**, while **3d** having 4-Br group revealed moderate activity against *P. vulgaris* (IZ = 17 mm) compared to gentamycin (IZ = 25 mm). On the other hand, compounds **5a**, **5b**, **5g** and **5h** displayed reasonable antibacterial activities against *P. vulgaris* with IZ values 16, 18, 17 and 18, respectively. Additionally, most compounds revealed mild antibacterial activities against the gram negative *E. coli*.

2.3.2. Antifungal activity

Most of the tested formazan analogues exhibited promising antifungal activities with the exception of **3e**, **5f** and **7b** that were inactive against used fungal strains.

Focusing on the antifungal activities of compounds **3a-e**, compound **3a** elicited comparable antifungal activity (IZ = 17 and 18 mm against *A. flavus* and *C. Albicans*, respectively) to ketoconazole (IZ = 16 and 20 mm against *A. flavus* and *C. Albicans*, respectively). Also, significant activities were observed for compounds **3b** and **3c** (IZ = 13–16 mm). In addition, compound **3d** demonstrated superior antifungal activity against *A. flavus* (Z = 20 mm) that was more potent than ketoconazole.

Furthermore, by studying the antifungal activities of **5a-h**, moderate to potent activities were displayed. Among these compounds, compound **5g** with 3-Cl group showed IZ = 20 mm against *A. flavus* and 18 mm against *C. Albicans* that were higher than those of ketoconazole. Additionally, compound **5a** showed comparble activity (IZ = 16 and 19 mm) to ketoconazole.

These antifungal activities results were highly appreciated since *A. fumigatus* is the second main cause of invasive aspergillosis and is the first leading cause of cutaneous aspergillosis [34]. In addition to the increased incidence of infections by *C. albicans*, the most common cause of candidiasis, and the increased resistance of *C. albicans* to antifungal drugs [35,36].

2.4. Docking study

2.4.1. Docking into Candida albicans leucyl-tRNA synthetase

Leucyl-tRNA synthetase (LeuRS) belongs to the family aminoacyl tRNA synthetases (aaRSs), group of central enzymes that play a crucial
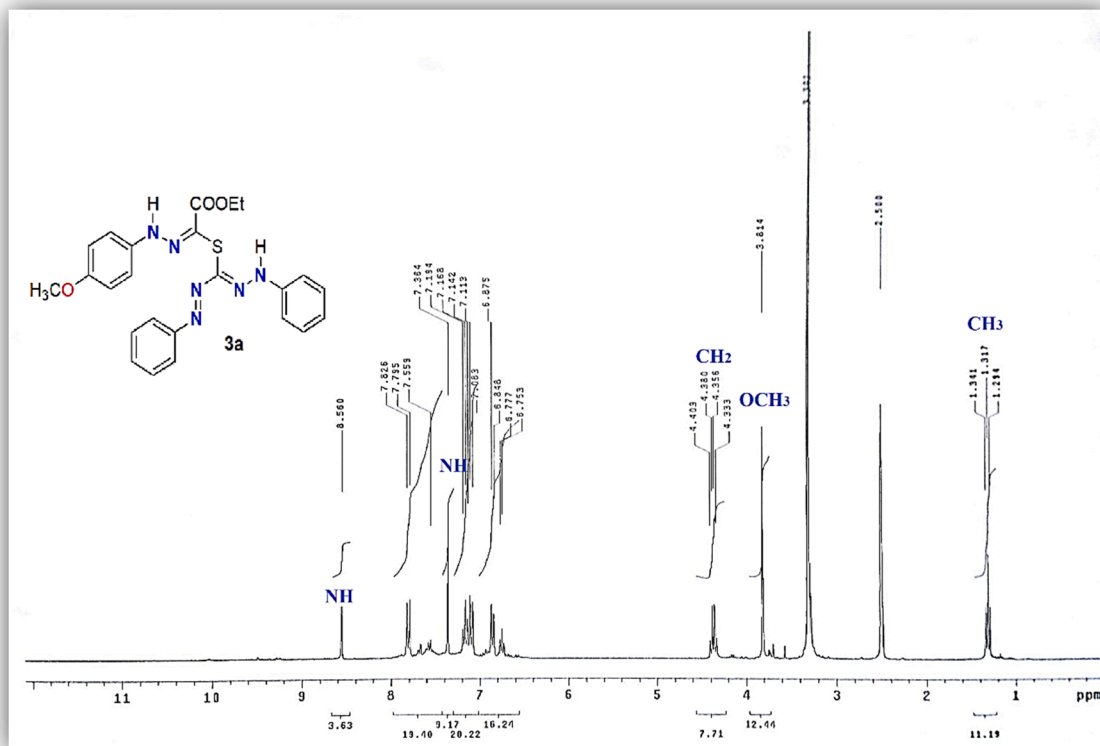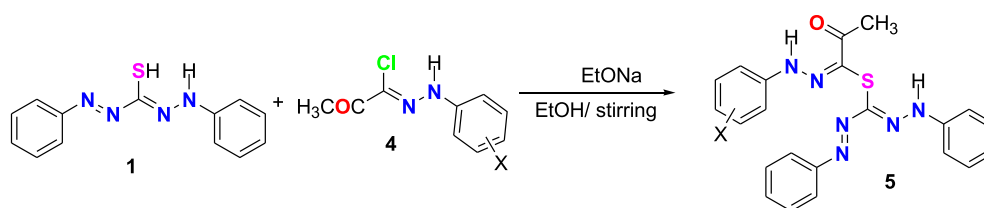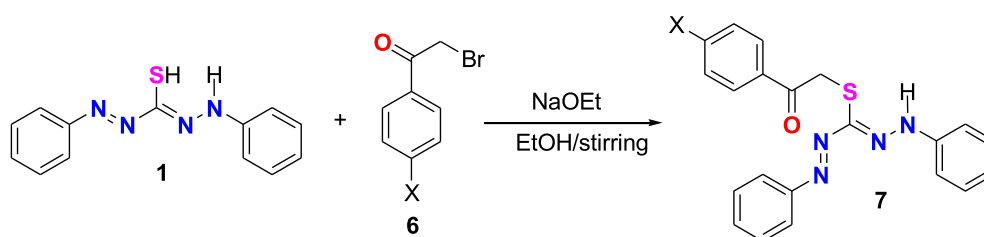
Fig. 3. The ^{1}H NMR spectrum of compound **3a**.

X: a, 4-OCH$_3$; b, 4-CH$_3$; c, H; d, 4-Cl; e, 4-NO$_2$; f, 3-CH$_3$; g, 3-Cl; h, 3-NO$_2$

Scheme 2. The reaction of dithiazone **1** with acetyl hydrazonoyl chlorides **4a-e**.

X: a, H; b, Cl

Scheme 3. The reaction of dithiazone **1** with phenacyl bromide derivative **6a-c**.

role in protein synthesis, which is vital for survival of micro-organism and hence its inhibition presented a novel and attractive target for developing antimicrobials [37]. Many recent reviews have discussed the importance of aaRSs in the discovery and development of antibacterial and antifungal agents [38-41].

In this study, molecular docking study of the newly synthesized formazan analogues **3a-f**, **5a-h** and **7a,b** have been performed onto the active site of *Candida albicans* editing domain of cytosolic leucyl-tRNA synthetase to demonstrate their binding affinity and orientation. MOE 2014 program was used for the docking simulation using cytosolic leucyl-tRNA synthetase editing domain cocrystallized with benzoxaborole-AMP adduct (PDB code: 2WFG). Docking of the cocrystallized ligand was done in order to validate the used docking method, it displayed docking score = −6.4725 Kcal/mol and RMSD = 0.654.
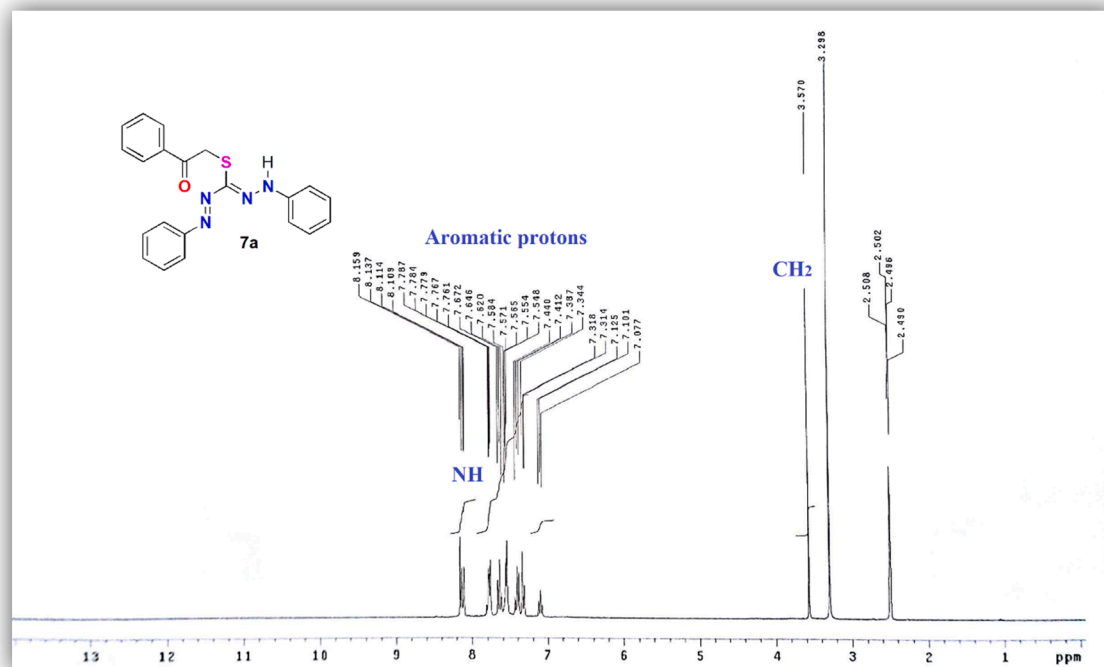
Fig. 4. The ^{1}H NMR spectrum of compound **7a**.
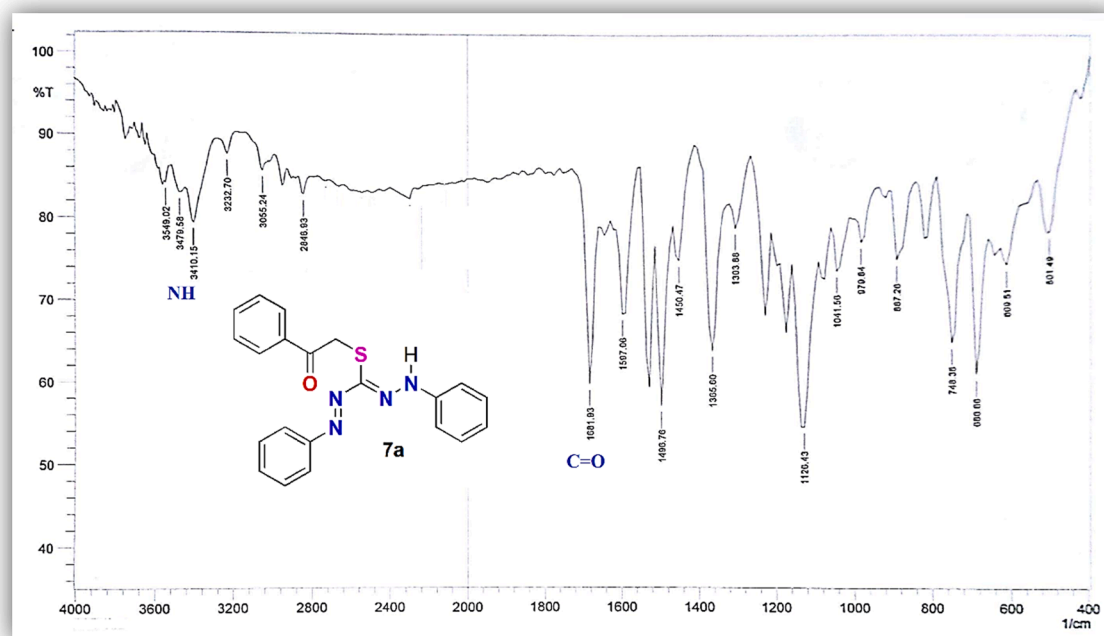
Fig. 5. The IR spectrum of derivative **7a**.

Results of the docking simulation were displayed in Table 4 showing the docking scores and the different formed interactions such as hydrogen bond, pi-H and non-polar pi-cation interactions.

For majority of compounds, Ala315, Lys407, and Lys483 were recognized as key amino acid residues responsible for hydrogen bonds generation and Thr316, Leu317, Arg318, Asp421 and Tyr487 were identified for minor interaction. Whereas, for pi-H and pi-cation interactions, Lys407, Ser419, Lys483 and Tyr487 were the only observed residues.

Focusing on the binding mode of the most active analogues as antifungals, **3a**, **3d**, **5a** and **5g** (Fig. 8), it was observed that they are well stabilized into the active site through strong hydrogen bonds and pi-H interactions with docking scores −7.8168, −7.4430, −7.5710 and −7.7562, respectively. The sulfur atom of **3a**, **3d** and **5a** formed hydrogen bond interactions with Ala315, while the hydrazonoyl nitrogen atoms were involved in hydrogen bonds with Lys407 and Lys483
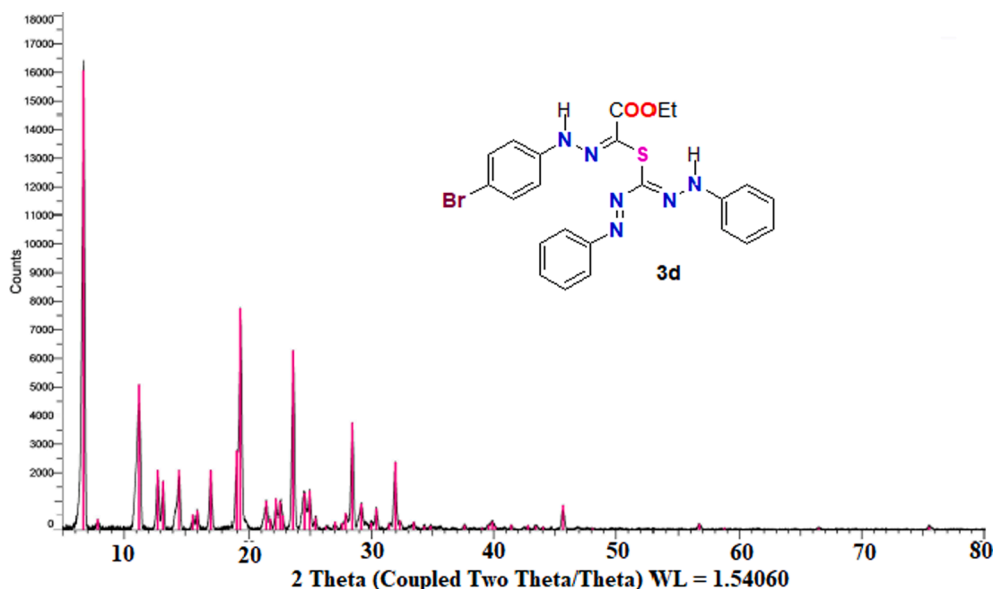
Fig. 6a. XRD Figures of formazan analogue **3d**.
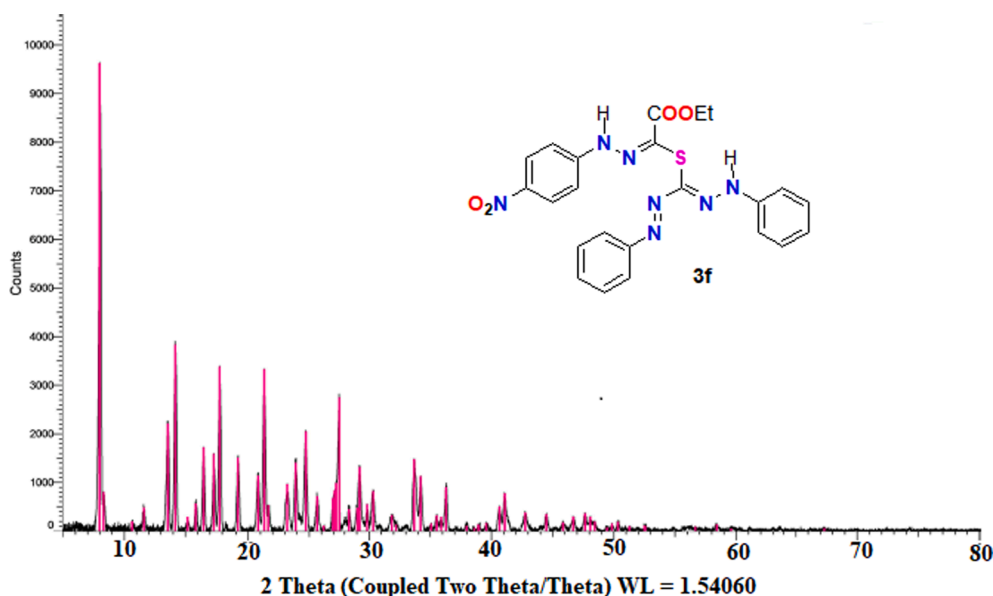
Fig. 6b. XRD Figures of formazan analogues **3f**.

residues. Additional hydrogen bond was seen between the hydrazonoyl nitrogen atom of **3a** and Thr316 and between **3d** and Leu317. Furthermore, the methoxy group of **5a** formed H-Pi interaction with Tyr487. For **5g**, three hydrogen bond interactions were observed between the hydrazonoyl nitrogen atoms and the important Leu317, Lys483 and Tyr487 residues.

2.4.2. Docking into COVID-19 3CLpro-2

Due to both the emergency of COVID-19 outbreak together with previous reports of the antiviral activities of formazan derivatives, we evaluated the antiviral potential of the synthesized formazan analogues against COVID-19 by targeting 3CLpro-2 through molecular docking.

The 3C-like protein (3CLpro-2) is the central protease of SARS-CoV-2. It plays a vital role in viral RNA translation and maturation and, thus, is critical for viral replication rendering it an attractive target for developing anti-coronavirus drug [6].

The protein structure of 3CLpro-2 consists of 9 α-helices and 13

β-strands making together three distinctive domains: Domain I (residues 8–101), Domain II (residues 102–184) and Domain III (residues 201–306) connected to Domain II by an extended loop (residues 185–200). 3CLpro-2 contains a catalytic dyad that is composed of conserved residues His41 and Cys145 and the key substrate-binding site is formed as a split between Domain I and Domain II [42].

To estimate the binding affinity of derivatives **3a-f**, **5a-h** and **7a,b** with COVID-19 3CLpro (PDB code: 6LU7), molecular docking study was done. As shown in Table 5, our newly synthesized compounds were found to fit deeply in the active site of COVID-19 3CL protease with binding energies ranging from −5.6064 to −8.0555 Kcal/mol. Interestingly, the key amino acid residue Cys145 was involved in hydrogen bond interactions with all of the tested compounds. Moreover, residues His41, Asn142, Gly143, His163, His164, and Gln189 were positively contributed in hydrogen bonding. While, Met49, Glu166 and Gln189 were contributed in the formed Pi-H interactions.

The analysis of the binding poses of compounds **3b**, **5b** and **5g** having
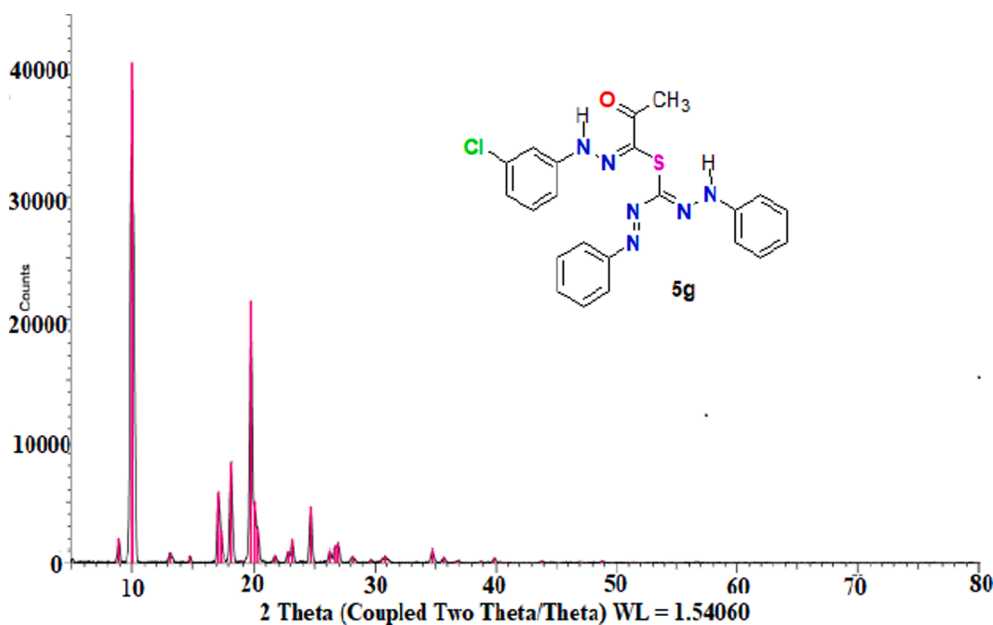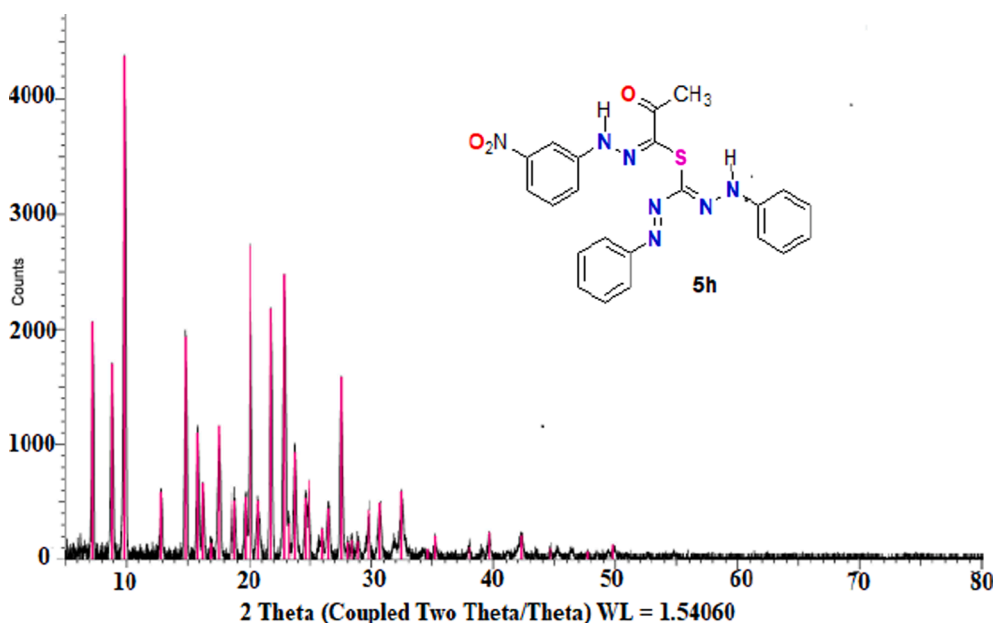
Fig. 6c. XRD Figures of formazan analogues **5g**.

Fig. 6d. XRD Figures of formazan analogues **5h**.

the best binding scores −7.7700, −8.0555 and −7.7868 Kcal/mol, respectively revealed closed binding pattern (Fig. 9). Concerning the ethyl ester formazan derivative **3b**, the sulfur atom formed hydrogen bond with Cys145, while the hydrazonoyl NH group is involved in hydrogen bonding with His164. Moreover, Pi-H interaction was observed between the tolyl phenyl moiety of **3b** and Glu166. On the other hand, the acetyl groups of **5b** and **5g** were bonded to His163 through hydrogen bonds. Additional hydrogen bonds connected **5b** and **5g** with His163 and His164 residues. Moreover, hydrophobic interactions were noticed between the tolyl moieties of **3b** and **5b**/the 3-chlorophenyl group of **5g** and Glu166, Pro168, Gln192 and Gln189 indicating the importance of these hydrophobic moieties.

3. Conclusion

Finally, we succeeded to synthesize a new series of nano-sized formazan analogues in excellent yield *via* the reaction of dithiazone with different types of hydrazonoyl chlorides and phenacyl bromide derivatives. Characterization of the crystal size and the structure of the formed formazan analogues were achieved with the aid of XRD, SEM and the spectral information. Evaluation of the antibacterial and antifungal activities demonstrated that most derivatives have mild or moderate antibacterial activity, while significant antifungal activity was observed for most compounds. Some derivatives like **3a**, **3d**, **5a** and **5g** displayed potent antifungal activity against tested fungal strains (IZ = 16–20 mm) compared to the reference drug ketoconazole (IZ = 16 and 20 mm against *A. flavus* and *C. Albicans*, respectively). Molecular modeling study revealed that these compounds could bind properly to
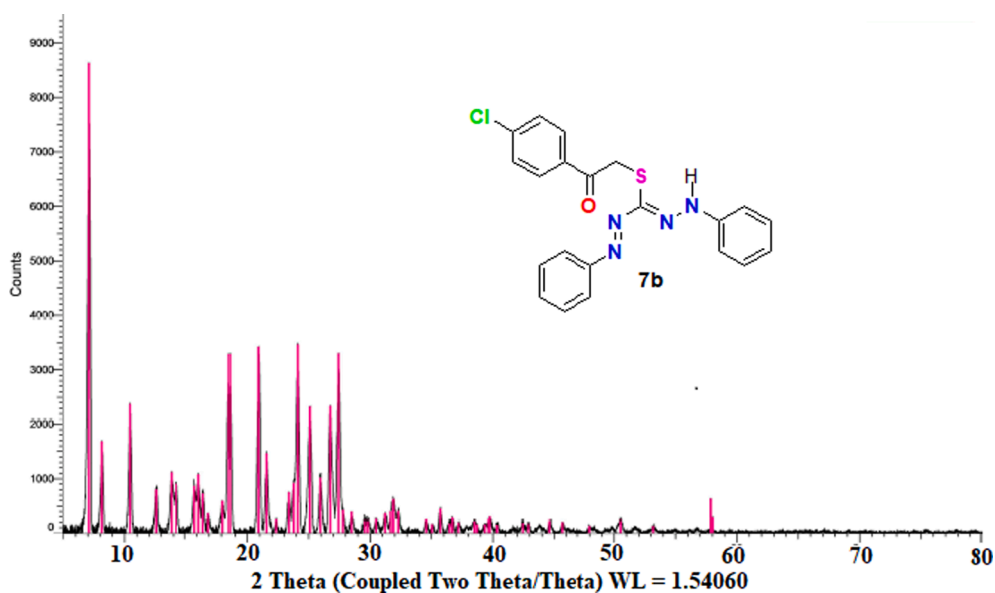
Fig. 6e. XRD Figures of formazan analogues **7b**.

7b

5h
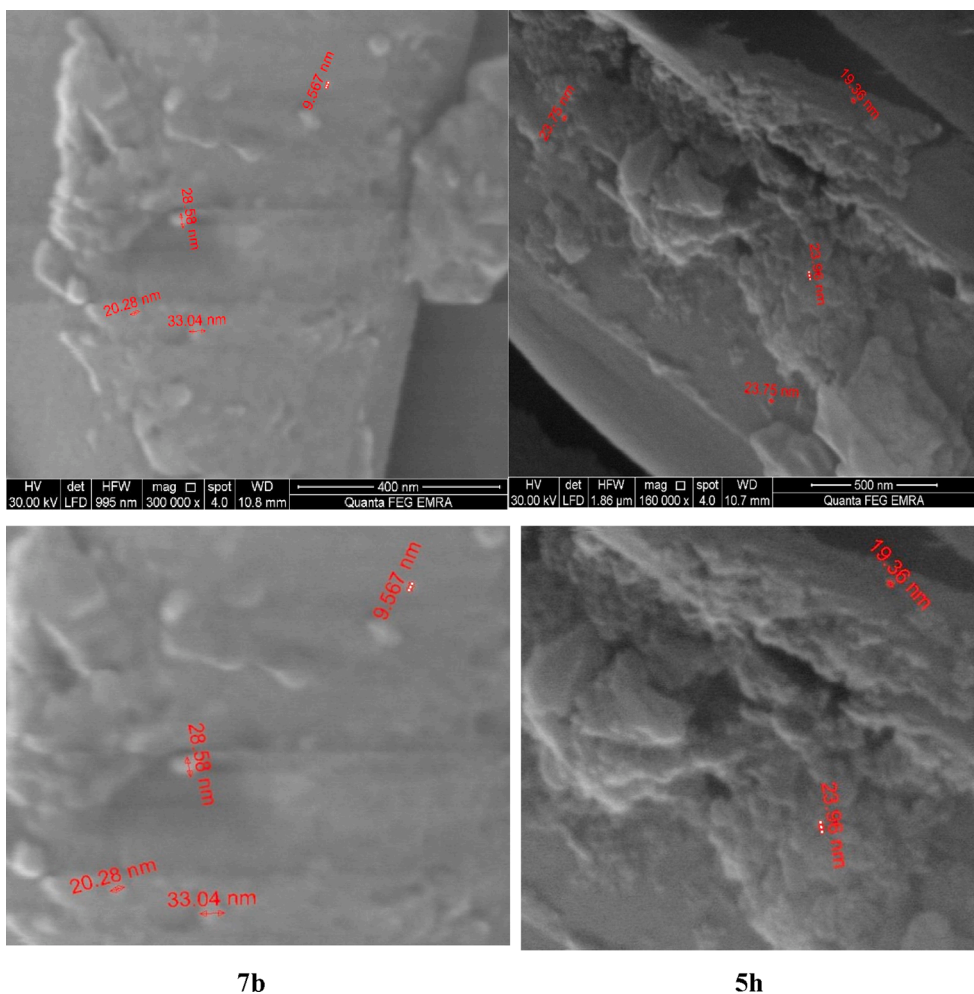
Fig. 7. Scanning electron micrographs images (SEM) of two derivatives of formazan analogues **5h** and **7b**.

C. albicans leucyl-tRNA synthetase editing domain. Additionally, docking simulation into the active site of COVID-19 3CL protease showed superior fitting into the active site with binding scores from −5.6064 to −8.0555 Kcal/mol.
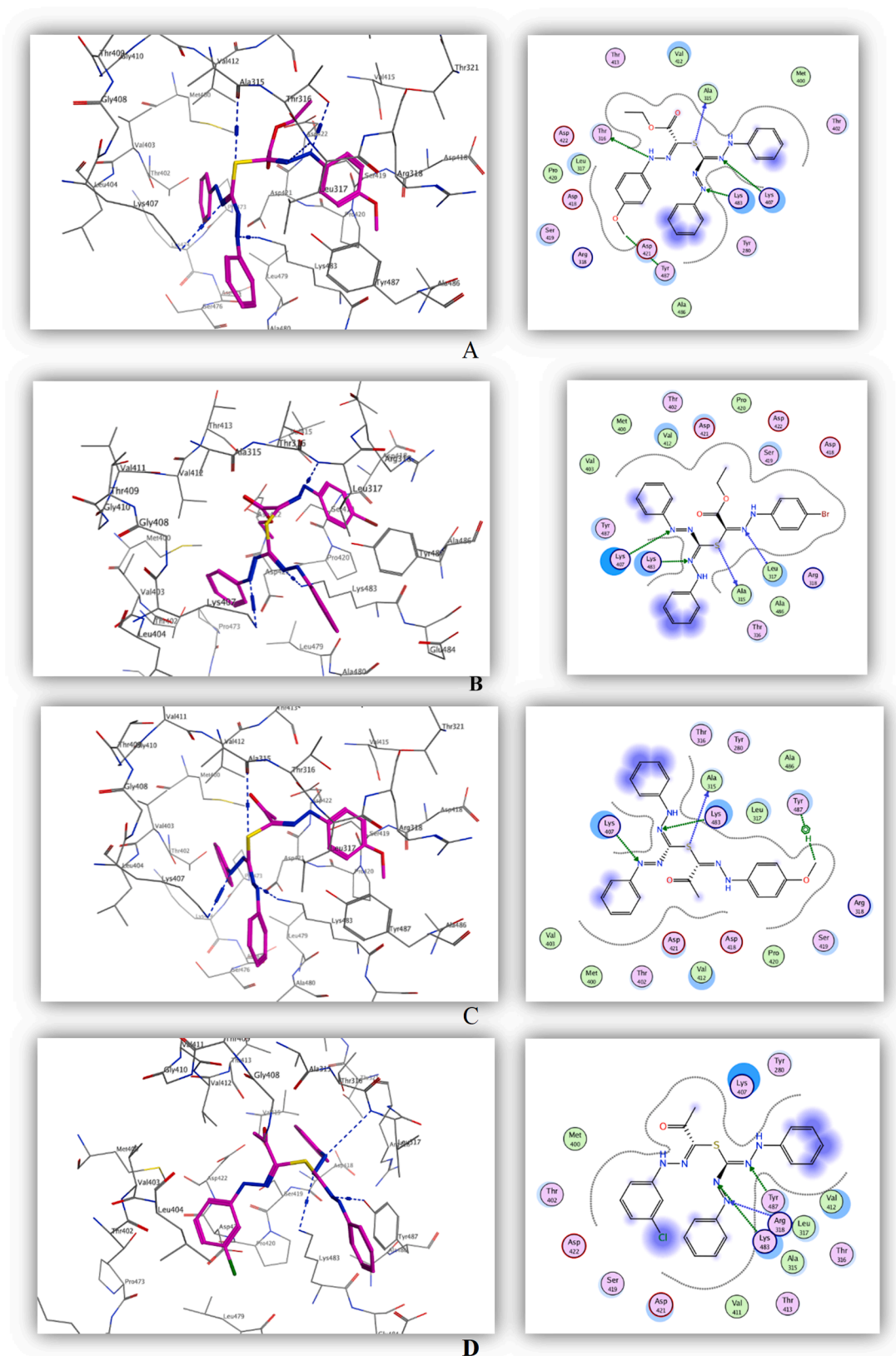
Fig. 8. The 3D and 2D proposed binding modes of **3a** (A), **3d** (B), **5a** (C) and **5g** (D) docked in the active site of leucyl-tRNA synthetase.
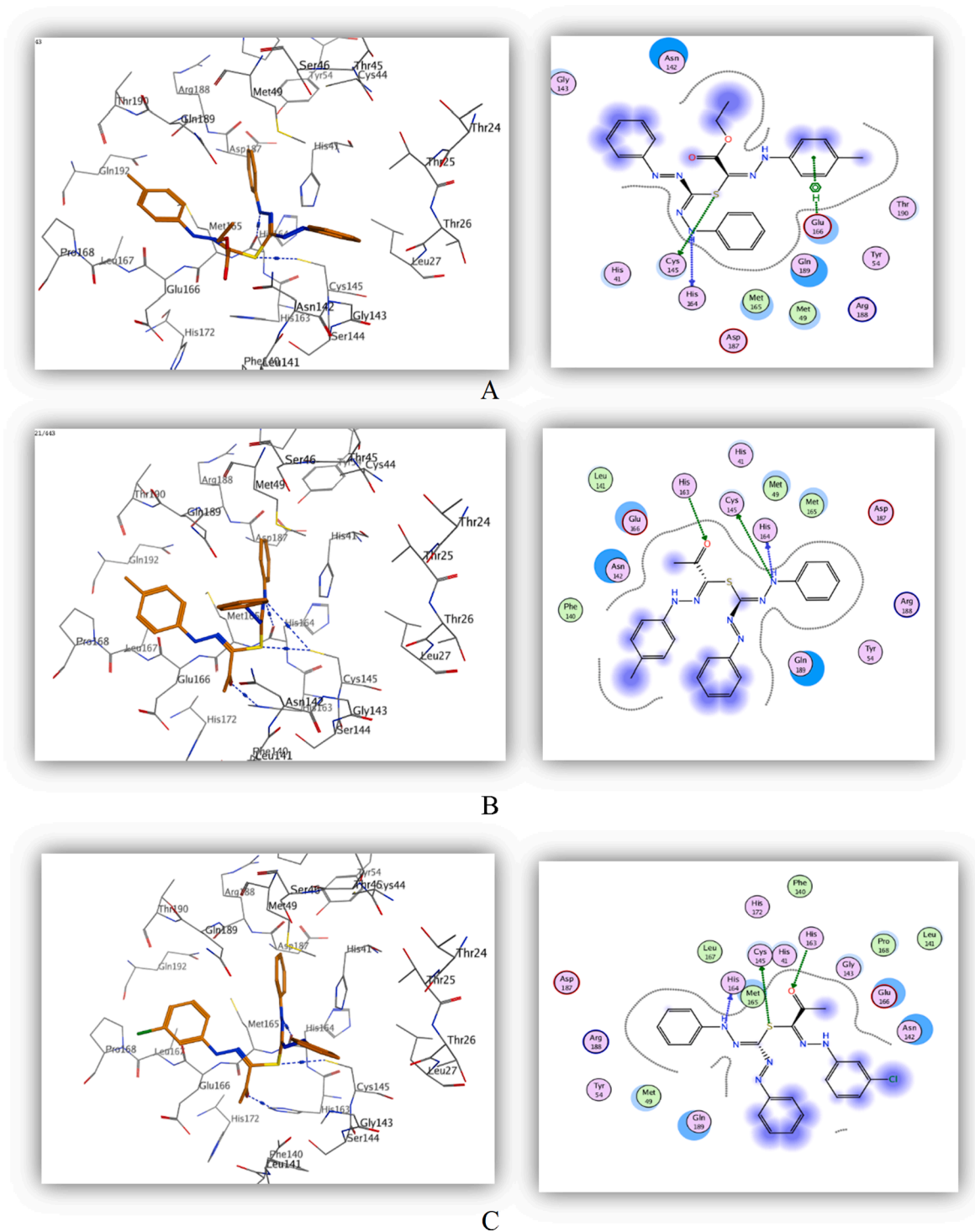
Fig. 9. The 3D and 2D proposed binding modes of **3b** (A), **5b** (B) and **5g** (C) docked in the active site of COVID-19 3CLpro.

Table 1
XRD parameters for nano-crystalline formazan analogues.

Compounds	Size (Å)	2θ	Intensity	d-spacing (Å)	FWHM
3d	7.172	6.686	16,068	13.21060	0.2022
3f	11.740	8.002	9628	11.04057	0.1236
5g	7.160	10.022	41,016	8.81878	0.2034
5h	14.088	9.845	4374	8.97683	0.1031
7b	23.356	7.103	8626	12.43540	0.0621

4. Experimental

4.1. General methods

The melting points of all new formazan analogues were recorded using a SMP3 melting point apparatus (the diameter of the glass capillaries is 0.5 mm). The 1430-Perkin-Elmer infrared-spectrophotometer was utilized to record the IR-spectra for all new formazan analogues in the range of wavenumber from 4000 cm^{-1} to 200 cm^{-1} as through the formation of sample-KBr discs. The well-known Bruker Avance-300

Table 2

Antifungal activity of the target compounds (**3a-e**, **5a-h** and **7a,b**) expressed as mean zones of inhibition in mm based on diffusion agar technique.

Sample code	Tested Fungi Microorganisms	
	Aspergillus flavus	*Candida albicans*
3a	17	18
3b	15	16
3c	13	14
3d	20	16
3e	NA	NA
5a	16	19
5b	15	13
5c	15	16
5d	15	14
5e	11	18
5f	NA	NA
5g	20	18
5h	15	13
7b	NA	NA
Ketoconazol	16	20

Table 3

Antibacterial activity of the target compounds (**3a-e**, **5a-h** and **7b**) expressed as mean zones of inhibition in mm based on diffusion agar technique.

Sample code	Tested bacteria Microorganisms			
	Gram Positive Bacteria:		Gram Negatvie Bacteria:	
	Staphylococcus aureus	*Bacillus subtilis*	*Escherichia coli*	*Proteus vulgaris*
3a	13	8	NA	NA
3b	14	NA	NA	NA
3c	13	14	12	14
3d	15	13	11	17
3e	10	NA	NA	11
5a	13	18	15	16
5b	15	18	15	18
5c	15	16	13	12
5d	12	15	12	13
5e	14	17	11	12
5f	8	14	13	12
5g	12	17	14	17
5h	15	18	15	18
7b	8	NA	NA	8
Gentamycin	24	26	30	25

Table 4

Docking results of the target compounds against *Candida albicans* leucyl-tRNA synthetase.

Compound	Docking score (kcal/mol)	Interacting residues (Type of interaction)	Distance (A⁰)
3a	−7.8168	Ala315 (H bond)	3.45
		Thr316 (H bond)	3.12
		Lys407 (H bond)	3.33
		Lys483 (H bond)	2.83
		Tyr487 (H-Pi)	4.29
3b	−7.3313	Ala315 (H bond)	3.20
		Lys407 (Pi-cation)	3.91
		Lys407 (Pi-cation)	4.29
		Tyr487 (H bond)	2.84
3c	−7.1818	Lys407 (H bond)	3.36
		Tyr487 (H bond)	2.90
3d	−7.4430	Ala315 (H bond)	3.48
		Leu317 (H bond)	3.24
		Lys407 (H bond)	3.26
		Lys483 (H bond)	2.83
3e	−6.5127	–	–
3f	−7.0200	Lys407 (Pi-cation)	4.00
		Tyr487 (H bond)	3.01
5a	−7.5710	Ala315 (H bond)	3.58
		Lys407 (H bond)	3.16
		Lys483 (H bond)	2.76
		Tyr487 (H-Pi)	4.34
5b	−7.1052	Ala315 (H bond)	3.46
		Lys407 (H bond)	3.28
		Lys483 (H bond)	2.80
5c	−7.0641	Lys407 (H bond)	3.28
		Ser419 (Pi-H)	4.40
		Lys483 (H bond)	3.18
		Tyr487 (H bond)	2.85
5d	−7.2187	Ala315 (H bond)	3.13
		Lys407 (Pi-cation)	3.89
		Lys407 (Pi-cation)	4.34
		Tyr487 (H bond)	2.87
5e	−7.4357	Ala315 (H bond)	3.71
		Arg318 (H bond)	3.44
		Lys407 (Pi-cation)	4.40
		Lys483 (Pi-H)	4.34
5f	−6.6872	Lys483 (H bond)	2.93
5g	−7.7562	Leu317 (H bond)	3.70
		Lys483 (H bond)	3.41
		Tyr487 (H bond)	2.88
5h	−6.3603	Lys483 (H bond)	3.03
7a	−6.0904	Ser419 (Pi-H)	3.95
7b	−6.1826	Asp421 (H bond)	3.16

instrument was utilized to record the ^{1}H NMR-spectra for all new formazan analogues at 300 MHz DMSO-d_6 solutions. Ppm and Hz characterize the chemical shifts (δ) and coupling constants, respectively. To record the molecular weight of all new formazan analogues we used a Finnigan-MAT8222 spectrometer at 70 eV in Micro-analytical center at Cairo University. Also, measuring of CHN elemental analyzes were investigated on Elementar vario-LIII C—H—N—S analyzer.

4.1.1. Synthesis of formazan analogues 3a-e, 5a-f, and 7a,b

To a stirred solution of 0.56 g of dithizone **1** (1 mmol) in sodium ethoxide solution (1 mmol of Na in 20 mL absolute EtOH) was added portion wise the suitable hydrazonyl chlorides **2a-f** or **4a-h** or the phenacyl derivatives **6a,b**, then the mixture was left to stirred for 2 h. The formed colored formazan analogues solid was filtered, washed with MeOH and recrystallized from the suitable solvent to give the corresponding formazan analogues **3a-f**, **5a-h** and **7a,b**, respectively.

4.1.2. 2-Ethoxy-N′-(4-methoxyphenyl)-2-oxoacetohydrazonic-N′,2-diphenyldiazenecarbo-hydrazonic thioanhydride (3a)

Orange solid, yield (0.42 g, 90%), mp 158–160 °C (ethanol /dioxane), IR ὑ: 3425, 3178 (2NH), 1681 (CO), 1579 (C=N), 1535, 1465, 1338, 1288, 1226, 1134, 1064 cm^{-1}. ^{1}H NMR (DMSO-d_6) 1.32 (t, $J = 8.4\ Hz$, 3H, CH$_2$CH$_3$), 3.81 (s, 3H, OCH$_3$), 4.36 (q, $J = 8.4\ Hz$, 2H, CH$_2$CH$_3$), 6.86–7.83 (m, 14H, Ar H), 7.36 (s, 1H, NH), 8.56 (s, 1H, NH).

M/z (%) 477 (M$^+$+1, 12), 476 (M$^+$, 6), 446 (54), 402 (3), 370 (74), 342 (4), 312 (3), 279 (4), 242 (2), 224 (5), 210 (10), 166 (55), 147 (12), 133 (9), 121 (45), 105 (27), 97 (10), 77 (100). Anal. Calcd. for C$_{24}$H$_{24}$N$_6$O$_3$S (476.55) Calcd: C, 60.49; H, 5.08; N, 17.64. Found: C, 60.62; H, 5.28; N, 17.45%.

4.1.3. 2-Ethoxy-2-oxo-N′-(p-tolyl)acetohydrazonic-N′,2-diphenyldiazenecarbohydrazonic thioanhydride (3b)

Orange solid, yield (0.39 g, 85%), mp 152–154 °C (ethanol /dioxane), IR ὑ: 3448, 3178 (2NH), 1681 (CO), 1597 (C=N), 1535, 1473, 1388, 1303, 1273, 1234. 1188, 1157, 1134. cm^{-1}. ^{1}H NMR (DMSO-d_6) 1.32 (t, 3H, CH$_2$CH$_3$), 2.26 (s, 3H, CH$_3$), 4.36 (q, 2H, CH$_2$CH$_3$), 6.76–7.83 (m, 14H, Ar H), 7.36 (s, 1H, NH), 8.59 (s, 1H, NH). Anal. Calcd. for C$_{24}$H$_{24}$N$_6$O$_2$S (460.55) Calcd: C, 62.59; H, 5.25; N, 18.25. Found: C, 62.39; H, 5.29; N, 18.16%.

4.1.4. 2-Ethoxy-2-oxo-N′-phenylacetohydrazonic-N′,2-diphenyldiazenecarbohydrazonic thioanhydride (3c)

Orange solid, yield (0.42 g, 95%), mp 138–140 °C (ethanol /dioxane), IR ὑ: 3446 (br2NH), 1671 (CO), 1601 (C=N), 1536, 1474, 1383, 1277, 1237, 1128, 1059 cm^{-1}. ^{1}H NMR (DMSO-d_6) 1.32 (t, 3H, CH$_2$CH$_3$), 4.39 (q, 2H, CH$_2$CH$_3$), 6.74–7.98 (m, 15H, Ar H), 7.39 (s, 1H, NH), 8.63 (s, 1H, NH). M/z (%) 448 (M$^+$+1, 0.63), 429 (19), 416 (14),

Table 5

Docking results of the target compounds against COVID-19 3CLpro.

Compound	Docking score (kcal/mol)	Interacting residues (Type of interaction)	Distance (A⁰)
3a	−7.2566	Met49 (Pi-H)	4.19
		Cys145 (H bond)	4.41
3b	−7.7700	Cys145 (H bond)	3.84
		His164 (H bond)	3.08
		Glu166 (Pi-H)	4.60
3c	−7.2756	His41 (H bond)	3.17
		Cys145 (H bond)	3.40
3d	−7.2122	Cys145 (H bond)	3.95
		Cys145 (H bond)	3.39
		His164 (H bond)	3.37
		Gln189 (H bond)	2.98
3e	−7.1521	Cys145 (H bond)	3.74
		His163 (H bond)	3.40
3f	−6.1250	Cys145 (H bond)	2.87
		Cys145 (H bond)	3.24
		Met165 (H bond)	4.11
5a	−7.3248	Asn142 (H bond)	3.18
		Asn142 (H bond)	2.97
		Cys145 (H bond)	3.95
		His164 (H bond)	3.03
		Glu166 (Pi-H)	4.66
5b	−8.0555	Cys145 (H bond)	3.35
		His163 (H bond)	3.33
		His164 (H bond)	3.40
5c	−7.1865	Cys145 (H bond)	3.74
		His163 (H bond)	3.28
5d	−7.0781	Cys145 (H bond)	3.13
		His164 (H bond)	2.92
		Gln189 (Pi-H)	3.95
5e	−7.3608	Cys145 (H bond)	3.74
		His163 (H bond)	3.31
5f	−5.6064	Gly143 (H bond)	2.85
		Cys145 (H bond)	3.95
5g	−7.7868	Cys145 (H bond)	3.56
		His163 (H bond)	3.26
		His164 (H bond)	3.12
5h	−5.9377	Gly143 (H bond)	3.20
		Cys145 (H bond)	3.68
7a	−6.9032	Cys145 (H bond)	4.13
		His164 (H bond)	3.9
7b	−6.4258	Cys145 (H bond)	3.91

243 (4), 208 (2), 195 (10), 183 (20), 167 (100), 152 (7), 118 (5), 105 (14), 91 (28), 77 (78). Anal. Calcd. for $C_{23}H_{22}N_6O_2S$ (446.52) Calcd: C, 61.87; H, 4.97; N, 18.82. Found: C, 61.77; H, 4.85; N, 18.64%.

4.1.5. *N′-(4-Bromophenyl)-2-ethoxy-2-oxoacetohydrazonic-N′,2-diphenyldiazenecarbo-hydrazonic thioanhydride (3d)*

Orange solid, yield (0.49 g, 90%), mp 162–164 °C (ethanol /dioxane), IR ύ: 3510, 3464 (2NH), 1674 (CO), 1604 (C=N), 1527, 1473, 1388, 1234, 1126, 1064, 1010 cm⁻¹. ¹H NMR (DMSO-d_6) 1.32 (t, 3H, CH$_2$CH$_3$), 4.37 (q, 2H, CH$_2$CH$_3$), 6.75–7.99 (m, 14H, Ar H), 7.36 (s, 1H, NH), 8.68 (s, 1H, NH). M/z (%) 525 (M⁺, 0.02),480 (1), 420 (19), 392 (2), 340 (13). 214 (4), 170 (7), 150 (4), 135 (4), 105 (29), 92 (35), 77 (100). Anal. Calcd. for $C_{23}H_{21}BrN_6O_2S$ (525.42) Calcd: C, 52.58; H, 4.03; N, 15.99. Found: C, 52.33; H, 4.22; N, 16.08%.

4.1.6. *2-Ethoxy-N′-(3-nitrophenyl)-2-oxoacetohydrazonic-N′,2-diphenyldiazenecarbo-hydrazonic thioanhydride (3e)*

Orange solid, yield (0.44 g, 90%), mp 252–254 °C (ethanol /dioxane), IR ύ: 3525, 3425 (2NH), 1743 (CO), 1589 (C=N), 1535, 1489, 1350, 1265, 1157, 1103, 1010 cm⁻¹. ¹H NMR (DMSO-d_6) 1.34 (t, 3H, CH$_2$CH$_3$), 4.39 (q, 2H, CH$_2$CH$_3$), 6.77–8.42 (m, 14H, Ar H), 8.78 (s, 1H, NH), 9.09 (s, 1H, NH). M/z (%) 492 (M⁺+1, 0.41), 491 (M⁺, 0.73), 474 (2), 393 (3), 368 (5), 354 (2), 339 (8), 313 (19), 292 (4), 264 (20), 239 (16), 183 (12), 167 (36), 152 (7), 135 (12), 129 (14), 123 (13), 109 (23), 95 (37), 83 (54), 77 (69), 69 (67), 57 (100). Anal. Calcd. for $C_{23}H_{21}N_7O_4S$ (491.52) Calcd: C, 56.20; H, 4.31; N, 19.95. Found: C,

56.33; H, 4.54; N, 19.76%.

4.1.7. *2-Ethoxy-N′-(4-nitrophenyl)-2-oxoacetohydrazonic-N′,2-diphenyldiazenecarbo-hydrazonic thioanhydride (3f)*

Dark red solid, yield (0.41 g, 85%), mp ˃ 300 °C (ethanol /dioxane), IR ύ: 3410, 3263 (2NH), 1728(CO), 1604 (C=N), 1496, 1458, 1357, 1288, 1234, 1149, 1080, 1056 cm⁻¹. ¹H NMR (DMSO-d_6). M/z (%) 492 (M⁺+1, 0.11), 491 (M⁺, 0.09), 310 (39), 282 (6), 221 (5), 177 (32), 150 (14), 135 (8), 119 (11), 108 (21), 105 (21), 93 (83), 77 (100). Anal. Calcd. for $C_{23}H_{21}N_7O_4S$ (491.52) Calcd: C, 56.20; H, 4.31; N, 19.95. Found: C, 56.23; H, 4.54; N, 19.86%.

4.1.8. *N′-(4-Methoxyphenyl)-2-oxopropanehydrazonic-N′,2-diphenyldiazenecarbo-hydrazonic thioanhydride (5a)*

Orange solid, yield (0.41 g, 93%), mp 140–142 °C (ethanol /dioxane), IR ύ: 3451 (br. 2NH), 1658 (CO), 1600 (C=N), 1533, 1481, 1460, 1386, 1269, 1228, 1190, 1156, 1129, 1020 cm⁻¹. ¹H NMR (DMSO-d_6) 2.36 (s, 3H, CH$_3$), 3.71 (s, 3H, OCH$_3$), 6.96–7.66 (m, 14H, Ar-H), 10.93 (s, 1H, NH), 11.30 (s, 1H, NH). M/z (%) 446 (M⁺, 1), 255 (0.36), 339 (6), 136 (1.2), 122 (45), 107 (16), 106 (10), 105 (31), 92 (43), 91 (8), 77 (100), 65 (28).Anal. Calcd. for $C_{23}H_{22}N_6O_2S$ (446.52) Calcd: C, 61.87; H, 4.97; N, 18.82. Found: C, 61.99; H, 4.88; N, 18.64%.

4.1.9. *2-Oxo-N′-(p-tolyl)propanehydrazonic-N′,2-diphenyldiazenecarbohydrazonic thioanhydride (5b)*

Orange solid, yield (0.38 g, 90%), mp 132–134 °C (ethanol /dioxane), IR ύ: 3452 (br. 2NH), 1649 (CO), 1601 (C=N), 1540, 1489, 1459, 1388, 1273, 1233, 1191, 1154, 1130, 1070, 1021 cm⁻¹. ¹H NMR (DMSO-d_6) 2.26 (s, 3H, CH$_3$), 2.38 (s, 3H, CH$_3$), 6.47–7.90 (m, 14H, Ar-H), 10.89 (s, 1H, NH), 11.40 (s, 1H, NH). M/z (%)432 (M⁺+2, 0.26), 310 (0.32), 223 (3), 175 (1.34), 120 (1.12), 118 (4), 106 (14), 105 (49), 92 (40), 91 (46), 77 (73), 65 (45). Anal. Calcd. for $C_{23}H_{22}N_6OS$ (430.53) Calcd: C, 64.16; H, 5.15; N, 19.52. Found: C, 64.23; H, 5.30; N, 19.45%.

4.1.10. *2-Oxo-N′-phenylpropanehydrazonic-N′,2-diphenyldiazenecarbohydrazonic thioanhydride (5c)*

Orange solid, yield (0.39 g, 95%), mp 156–158 °C (ethanol /dioxane), IR ύ: 3449 (br. 2NH), 1662 (CO), 1598 (C=N), 1534, 1474, 1439, 1382, 1249, 1269, 1228, 1190, 1150, 1127, 1070, 1020 cm⁻¹. ¹H NMR (DMSO-d_6) 2.37 (s, 3H, CH$_3$), 7.07–7.63 (m, 15H, Ar-H), 10.93 (s, 1H, NH), 11.26 (s, 1H, NH). M/z (%)416 (M⁺, 0.36), 339 (4), 223 (2), 161 (0.5), 150 (14), 105 (52), 92 (31), 77 (100), 65 (27). Anal. Calcd. for $C_{22}H_{20}N_6OS$ (416.50) Calcd: C, 63.44; H, 4.84; N, 20.18. Found: C, 63.23; H, 4.65; N, 20.22%.

4.1.11. *N′-(4-Chlorophenyl)-2-oxopropanehydrazonic-N′,2-diphenyldiazenecarbohydrazonic thioanhydride (5d)*

Orange solid, yield (0.4 g, 90%), mp 146–148 °C (ethanol /dioxane), IR ύ: 3451 (br. 2NH), 1657 (CO), 1597 (C=N), 1535, 1486, 1464, 1381, 1337, 1269, 1228, 1189, 1156, 1131, 1021 cm⁻¹. ¹H NMR (DMSO-d_6) 1.60 (s, 3H, CH$_3$), 7.11–7.93 (m, 14H, Ar-H), 10.92 (s, 1H, NH), 11.58 (s, 1H, NH). M/z (%)452 (M⁺+2, 0.15), 451 (M⁺+1, 0.09), 450 (M⁺, 0.27), 346 (12), 344 (31), 228 (2), 139 (1.8), 126 (16), 111 (12), 106 (5), 105 (30), 92 (52), 91 (9), 77 (100), 65 (28). Anal. Calcd. for $C_{22}H_{19}ClN_6OS$ (450.94) Calcd: C, 58.60; H, 4.25; N, 18.64. Found: C, 58.88; H, 4.45; N, 18.45%.

4.1.12. *N′-(4-Nitrophenyl)-2-oxopropanehydrazonic-N′,2-diphenyldiazenecarbohydrazonic thioanhydride (5e)*

Orange solid, yield (0.39 g, 85%), mp ˃ 300 °C (ethanol /dioxane), IR ☐: 3479 (br. 2NH), 1662 (CO), 1596 (C=N), 1536, 1503, 1479, 1422, 1384, 1336, 1266, 1228, 1186, 1170, 1127, 1072, 1021 cm⁻¹. ¹H NMR (DMSO-d_6) 1.94 (s, 3H, CH$_3$), 7.0–8.28 (m, 14H, Ar-H), 11.20 (s, 1H, NH), 11.47 (s, 1H, NH). M/z (%)461 (M⁺, 0.18), 310 (1.9), 255 (1.1), 206 (0.74), 137 (3.5), 122 (1.7), 106 (9), 105 (27), 92 (64), 91 (11), 77 (100), 65 (40). Anal. Calcd. for $C_{22}H_{19}N_7O_3S$ (461.50) Calcd: C, 57.26;

H, 4.15; N, 21.25. Found: C, 57.34; H, 4.26; N, 21.19%.

4.1.13. 2-Oxo-N′-(m-tolyl)propanehydrazonic-N′,2-diphenyldiazenecarbohydrazonic thioanhydride (5f)

Orange solid, yield (0.36 g, 85%), mp 144–146 °C (ethanol /dioxane), IR ύ: 3436 (br 2NH), 1653 (CO), 1594 (C=N), 1536, 1472, 1378, 1269, 1194, 1129, 1027 cm^{-1}. ^{1}H NMR (DMSO-d_6) 1.88 (s, 3H, CH$_3$), 2.19 (s, 3H, CH$_3$), 6.50–7.51 (m, 14H, Ar-H), 9.62 (s, 1H, NH), 10.65 (s, 1H, NH). M/z (%) 431 (M$^+$ +1, 0.14), 430 (M$^+$, 0.44), 324 (40), 310 (9), 222 (3), 194 (1), 166 (3), 150 (20), 132 (8), 106 (43), 92 (44), 77 (100). Anal. Calcd. for C$_{23}$H$_{22}$N$_6$OS (430.53) Calcd: C, 64.16; H, 5.15; N, 19.52. Found: C, 64.28; H, 5.36; N, 19.47%.

4.1.14. N′-(3-Chlorophenyl)-2-oxopropanehydrazonic-N′,2-diphenyldiazenecarbohydrazonic thioanhydride (5g)

Orange solid, yield (0.38 g, 85%), mp 160–162 °C (ethanol /dioxane), IR ύ: 3437 (br 2NH), 1659 (CO), 1593 (C=N), 1534, 1467, 1387, 1270, 1223, 1187, 1129, 1024 cm^{-1}. ^{1}H NMR (DMSO-d_6) 2.49 (s, 3H, CH$_3$), 6.78–8.22 (m, 14H, Ar-H), 7.36 (s, 1H, NH), 8.70 (s, 1H, NH). M/z (%) 452 (M$^+$+2, 0.16), 451 (M$^+$+1, 0.11), 450 (M$^+$, 0.38), 420 (3), 344 (28), 310 (7), 167 (4), 150 (8), 126 (16), 111 (9), 105 (35), 92 (60), 77 (100). Anal. Calcd. for C$_{22}$H$_{19}$ClN$_6$OS (450.94) Calcd: C, 58.60; H, 4.25; N, 18.64. Found: C, 58.58; H, 4.37; N, 18.52%.

4.1.15. N′-(3-Nitrophenyl)-2-oxopropanehydrazonic-N′,2-diphenyldiazenecarbohydrazonic thioanhydride (5h)

Red solid, yield (0.39 g, 85%), mp 164–166 °C (ethanol /dioxane), IR □: 3430 (br 2NH), 1661 (CO), 1595 (C=N), 1531, 1473, 1361, 1272, 1219, 1183, 1130, 1020 cm^{-1} ^{1}H NMR (DMSO-d_6) 2.49 (s, 3H, CH$_3$), 6.79–8.49 (m, 14H, Ar-H), 8.77 (s, 1H, NH), 9.19 (s, 1H, NH). M/z (%) 461 (M$^+$, 0.18), 431 (3), 355 (65), 208 (2), 181 (18), 167 (4), 150 (7), 118 (4), 105 (27), 92 (64), 77 (100). Anal. Calcd. for C$_{22}$H$_{19}$N$_7$O$_3$S (461.50) Calcd: C, 57.26; H, 4.15; N, 21.25. Found: C, 57.19; H, 4.31; N, 21.36%.

4.1.16. 2-Oxo-2-phenylethyl N′,2-diphenyldiazenecarbohydrazonothioate (7a)

Red solid, yield (0.31 g, 85%), mp 180–182 °C (ethanol /dioxane), IR □: 3410 (NH), 1681 (CO), 1597 (C=N), 1496, 1450, 1365, 1303, 1126, 1041 cm^{-1}. ^{1}H NMR (DMSO-d_6) 3.57 (s, 2H, CH$_2$), 7.08–8.14 (m, 15H, Ar-H), 8.15 (s, 1H, NH). M/z (%) 375 (M$^+$+1, 0.03), 374 (M$^+$, 0.14), 267 (21), 207 (0.46), 163 (0.32), 152 (0.59), 109 (0.98), 105 (29), 77 (100). Anal. Calcd. for C$_{21}$H$_{18}$N$_4$OS (374.46) Calcd: C, 67.36; H, 4.85; N, 14.96. Found: C, 67.45; H, 4.66; N, 14.72%.

4.1.17. 2-(4-Chlorophenyl)-2-oxoethyl N′,2-diphenyldiazenecarbohydrazonothioate (7b)

Red solid, yield (0.34 g, 85%), mp 190–192 °C (ethanol /dioxane), IR □: 3424 (NH), 1682 (CO), 1590 (C=N), 1524, 1490, 1360, 1303, 1229, 1173, 1130 cm^{-1}. ^{1}H NMR (DMSO-d_6) 3.80 (s, 2H, CH$_2$), 7.10–8.15 (m, 15H, Ar-H, NH). M/z (%) 409 (M$^+$+1, 0.08), 408 (M$^+$, 0.27), 267 (23), 139 (4), 113 (2), 111 (6), 105 (26), 77 (100). Anal. Calcd. for C$_{21}$H$_{17}$ClN$_4$OS (408.90) Calcd: C, 61.68; H, 4.19; N, 13.70. Found: C, 61.89; H, 4.34; N, 13.88%.

4.2. Antimicrobial activity assay

All the microbial strains that used in the current study have been supplied from Al-Azhar University in Cairo, Egypt from the culture collection of the Regional Center for Mycology and Biotechnology (RCMB). The method used for recording the antimicrobial activity according to the literature method [43].

5. Docking study

Molecular docking was analyzed through using MOE-Dock 2014

software [44]. Chemical structures of **3a-f**, **5a-h** and **7a,b** were drawn by the MOE builder followed by minimization using the force field MMFF94x in this program. Hydrogen atoms were then added and unwanted water molecules were cancelled. Docking was then performed using London dG for rescoring 1 and GBVI/WSA dG for rescoring 2. At the same time, refinement was done through forcefield. "Ligand Interactions" was utilized for the 2D visualization o the protein–ligand interactions. The best pose was then selected depending on the binding energy and the interactions found in the active site.

Declaration of Competing Interest

The authors declare that they have no known competing financial interests or personal relationships that could have appeared to influence the work reported in this paper.

References

[1] WHO Report on Surveillance of Antibiotic Consumption, 2018. https://www.who.int/medicines/areas/rational_use/oms-amr-amc-report-2016-2018/en/.

[2] J.S. Pham, K.L. Dawson, K.E. Jackson, E.E. Lim, C.F.A. Pasaje, K.E.C. Turner, S. A. Ralph, Aminoacyl-tRNA synthetases as drug targets in eukaryotic parasites, Int. J. Parasitol.: Drugs Drug Resistance 4 (1) (2014) 1–13, https://doi.org/10.1016/j.ijpddr.2013.10.001.

[3] F.L. Rock, W. Mao, A. Yaremchuk, M. Tukalo, T. Crepin, H. Zhou, Y.-K. Zhang, V. Hernandez, T. Akama, S.J. Baker, J.J. Plattner, L. Shapiro, S.A. Martinis, S. J. Benkovic, S. Cusack, M.R.K. Alley, An antifungal agent inhibits an aminoacyl-tRNA synthetase by trapping tRNA in the editing site, Science 316 (5832) (2007) 1759–1761, https://doi.org/10.1126/science.1142189.

[4] E. Seiradake, W. Mao, V. Hernandez, S.J. Baker, J.J. Plattner, M.R.K. Alley, S. Cusack, Crystal structures of the human and fungal cytosolic leucyl-tRNA synthetase editing domains: a structural basis for the rational design of antifungal benzoxaboroles, J. Mol. Biol. 390 (2) (2009) 196–207, https://doi.org/10.1016/j.jmb.2009.04.073.

[5] https://www.who.int/news-room/detail/27-04-2020-who-timeline—covid-19.

[6] P. Calligari, S. Bobone, G. Ricci, A. Bocedi, Molecular investigation of SARS–CoV-2 proteins and their interactions with antiviral drugs. Viruses 12 (2020) 445. doi: 10.3390/v12040445.

[7] D. Gentile, V. Patamia, A. Scala, M.T. Sciortino, A. Piperno, A. Rescifina. Putative inhibitors of SARS-CoV-2 main protease from a library of marine natural products: a virtual screening and molecular modeling study. Mar. Drugs 18 (2020) 225; doi: 10.3390/md18040225.

[8] O. Aly, Molecular docking reveals the potential of aliskiren, dipyridamole, mopidamol, rosuvastatin, rolitetracycline and metamizole to inhibit COVID-19 virus main protease, ChemRxiv (2020), https://doi.org/10.26434/chemrxiv.12061302.v1.

[9] M. Hoffmann et al., TMPRSS2 and Is Blocked by a Clinically Proven Protease Inhibitor. Cell (2020), 181, 271–280. doi: 10.1016/j.cell.2020.02.052.

[10] A.S. Shawali, N.A. Samy, Functionalized formazans: A review on recent progress in their pharmacological activities, J. Adv. Res. 6 (3) (2015) 241–254, https://doi.org/10.1016/j.jare.2014.07.001.

[11] P. Thangavelu, S. Cellappa, S. Thangavel, Synthesis, evaluation and docking studies of novel formazan derivatives as an enoyl-ACP reductase inhibitors, Int. J. Pharm. Pharm. Sci. 10 (2018) 56–61, https://doi.org/10.22159/ijpps.2018v10i8.26819.

[12] S.B. Chavan, S.B. Zangade, A.Y. Vibhute, Y.B. Vibhute, Synthesis and evaluation of antimicrobial activity of some new Schiff bases and formazans, Res. J. Pharm. Biol. Chem. Sci. 3 (2012) 262–269.

[13] J.P. Raval, P.R. Patel, N.H. Patel, P.S. Patel, V.D. Bhatt, K.N. Patel, Synthesis, characterization and in vitro antibacterial activity of novel 3-(4-methoxyphenyl)-1-isonicotinoyl-5-(substituted phenyl)-formazans, Intern. J. Chem. Tech. Res. 1 (2009) 610–615.

[14] B.C. Revanasiddappa, E.V.S. Subrahmanyam, Synthesis and biological studies of some novel formazans, Oriental J. Chem. 26 (2010) 243–246.

[15] D.D. Mukerjee, S.K. Shukla, B.L. Chowdhary, Synthesis of Some New Formazans as Potential Antiviral Agents, Arch. Pharm. Pharm. Med. Chem. 314 (12) (1981) 991–994.

[16] M.M. Tiwari, M. Agarwal, V.K. Saxena, S.K. Bajpai, M.M. Joshi, Synthesis and antiviral activity of some new formazans, Indian J. Pharm. Sci. 57 (1995) 113–116.

[17] V.K. Pandey, H.S. Negi, Synthesis of 1-(20aryl-40-oxo-3Hquinazolyl)-3-aryl-5-phenyl-formazans as potential anti-viral agents, Indian Drugs 36 (1990) 37–40.

[18] S.D. Bharadwaj, Synthesis of some new formazans and their biological activity, Int. J. Chem. Sci. 1 (2003) 272–277.

[19] R. Kalsi, K. Pande, T.N. Bhalla, S.S. Parmar, J.P. Barthwal, Novel formazans as potent anti-inflammatory and analgesic agents, Pharmacology 37 (1988) 218–224, https://doi.org/10.1159/000138469.

[20] R. Kalsi, K. Pande, T.N. Bhalla, J.P. Barthwal, G.P. Gupta, S.S. Parmar, Anti-Inflammatory Activity of Quinazolinoformazans, J. Pharm. Sci. 79 (4) (1990) 317–320, https://doi.org/10.1002/jps.2600790409.

[21] V.S. Misra, S. Dhar, B.L. Chowdhary, Synthesis of some newer formazans and tetrazolium salts as antiviral agents, Pharmazie 33 (1978) 790–792. PMID: 746062.

[22] V.S. Misra, S. Dhar, Synthesis of some newer formazans and tetrazolium salts and their effect on Ranikhet disease virus and the vaccinia virus, Pharmazie 35 (1980) 585–586. PMID: 7454738.

[23] N. Lakshmi, V. Haritha, V. Sreeram, D. Rajalakshm, N. Sindhura, D. Visagaperumal, Synthesis and their possible biological activities of few formazans of 3-amino-2-sulphanyl-2,3,4,5,6,7,8-hexahydrobenzothieno-[2,3-d] pyrimidin-4(1H)-one, Rasayan J. Chem. 2 (2009) 71–74.

[24] G. Uraz, E. Yilmaz, H. Tezcan, N. Porsuk, G. Imamoglu, O.S. Kartli, Synthesis and antimicrobial effects of 1,3,5-substituted phenylformazans, Asian J. Chem. 24 (2012) 1924–1926.

[25] N.G. Kandile, H.T. Zaky, M.I. Mohamed, H.M. Mohamed, Bull Korean Chem. Soc. 31 (2010) 3530.

[26] J. Li, D. Guo, X. Wang, H. Wang, H. Jiang, B. Chen, Nanoscale Res. Lett. 5 (2010) 1063.

[27] T.A. Farghaly, G.S. Masaret, Z.A. Muhamm, M.F. Harras, Discovery of thiazole-based-chalcones and 4-hetarylthiazoles as potent anticancer agents: Synthesis, docking study and anticancer activity, Bioorg. Chem. 98 (2020), 103761.

[28] A.F. Kassem, E.M.H. Abbas, N.T. Al-Qurashi, T.A. Farghaly, New azoloazine derivatives as antimicrobial agents: Synthesis under microwave irradiations, structure elucidation, and antimicrobial activity, J. Heterocyclic Chem. 57 (2) (2020) 611–620.

[29] I. Althagafi, N. El-Metwaly, T.A. Farghaly, New series of thiazole derivatives: Synthesis, structural elucidation, antimicrobial activity, molecular modeling and MOE docking, Molecules 24 (2019) 1741.

[30] D.H. Dawood, E.M.H. Abbas, T.A. Farghaly, M.M. Ali, M.F. Ibrahim, ZnO Nanoparticles catalyst in Synthesis of Bioactive Fused Pyrimidines as Anti-breast Cancer Agents Targeting VEGFR-2, Med. Chem. 15 (3) (2019) 277–286.

[31] A.M. Gouda, H.A. El-Ghamry, T.M. Bawazeer, T.A. Farghaly, A.N. Abdalla, A. Aslam, Antitumor activity of pyrrolizines and their Cu(II) complexes: Design, synthesis and cytotoxic screening with potential apoptosis-inducing activity, Eur. J. Med. Chem. 145 (2018) 350–359.

[32] T.A. Farghaly, M.A. Abdallah, G.S. Masaret, Z.A. Muhammad, New and efficient approach for synthesis of novel bioactive [1,3,4]thiadiazoles incorporated with 1,3-thiazole moiety, Eur. J. Med. Chem. 97 (2015) 320–333.

[33] Cullity, B. D.; Elements of X-ray Diffraction, second ed.Addison-Wesley, Massachusetts, 1978.

[34] M.T. Hedayati, A.C. Pasqualotto, P.A. Warn, P. Bowyer, D.W. Denning, Aspergillus flavus: human pathogen, allergen and mycotoxin producer, Microbiology 153 (6) (2007) 1677–1692, https://doi.org/10.1099/mic.0.2007/007641-0.

[35] D.K. Singh, R. Tóth, A. Gácser, Mechanisms of pathogenic candida species to evade the host complement attack, Front. Cell. Infect. Microbiol. 10 (2020) 94, https://doi.org/10.3389/fcimb.2020.00094.

[36] N. Mishra, T. Prasad, N. Sharma, A. Payasi, R. Prasad, D. Gupta, R. Singh, Pathogenicity and drug resistance in Candida albicans and other yeast species, Acta Microbiol. Immunol. Hung. 54 (3) (2007) 201–235, https://doi.org/10.1556/AMicr.54.2007.3.1.

[37] U.P. Singh, H.R. Bhat, P. Gahtori, R.K. Singh, Hybrid phenylthiazole and 1,3,5-triazine target cytosolic leucyl-tRNA synthetase for antifungal action as revealed by molecular docking studies, In Silico Pharmacol. 1 (1) (2013), https://doi.org/10.1186/2193-9616-1-3.

[38] S. Kim, S.W. Lee, E.-C. Choi, S.Y. Choi, Aminoacyl-tRNA synthetases and their inhibitors as a novel family of antibiotics, Appl. Microbiol. Biotechnol. 61 (4) (2003) 278–288, https://doi.org/10.1007/s00253-003-1243-5.

[39] U.A. Ochsner, X. Sun, T. Jarvis, I. Critchley, N. Janjic, Aminoacyl-tRNA synthetases: essential and still promising targets for new anti-infective agents, Expert Opin. Invest. Drugs 16 (5) (2007) 573–593, https://doi.org/10.1517/13543784.16.5.573.

[40] G.H.M. Vondenhoff, A. Van Aerschot, Aminoacyl-tRNA synthetase inhibitors as potential antibiotics, Eur. J. Med. Chem. 46 (11) (2011) 5227–5236, https://doi.org/10.1016/j.ejmech.2011.08.049.

[41] P.C. Lv, H.L. Zhu, Aminoacyl-tRNA synthetase inhibitors as potent antibacterials, Curr. Med. Chem. 19 (2012) 3550–3563, https://doi.org/10.2174/092986712801323199.

[42] P. Sang, S.-H. Tian, Z.-H. Meng, L.-Q. Yang, Anti-HIV drug repurposing against SARS-CoV-2, RSC Adv. 10 (27) (2020) 15775–15783, https://doi.org/10.1039/d0ra01899f.

[43] M.A. Pfaller, L. Burmeister, M.A. Bartlett, M.A. Ghorab, M.G. Rinaldi, J. Clin. Microbiol. 26 (1988) 1437–1441.

[44] Molecular Operating Environment (MOE) 2014.09, Chemical Computing Group Inc., 1010 Sherbrooke Street West, Suite 910, Montréal, H3A 2R7, Canada, http://www.chemcomp.com.